Rethinking the Ocean's Role in the Southern Oscillation

AMY CLEMENT

Rosenstiel School of Marine and Atmospheric Science, University of Miami, Miami, Florida

PEDRO DINEZIO

Rosenstiel School of Marine and Atmospheric Science, and Cooperative Institute for Marine and Atmospheric Studies, University of Miami, Miami, Florida

CLARA DESER

National Center for Atmospheric Research, Boulder, Colorado

(Manuscript received 4 August 2010, in final form 27 January 2011)

ABSTRACT

The Southern Oscillation (SO) is usually described as the atmospheric component of the dynamically coupled El Niño–Southern Oscillation phenomenon. The contention in this work, however, is that dynamical coupling is not required to produce the SO. Simulations with atmospheric general circulation models that have varying degrees of coupling to the ocean are used to show that the SO emerges as a dominant mode of variability if the atmosphere and ocean are coupled only through heat and moisture fluxes. Herein this mode of variability is called the thermally coupled Walker (TCW) mode. It is a robust feature of simulations with atmospheric general circulation models (GCMs) coupled to simple ocean mixed layers. Despite the absence of interactive ocean dynamics in these simulations, the spatial patterns of sea level pressure, surface temperature, and precipitation variability associated with the TCW are remarkably realistic. This mode has a red spectrum indicating persistence on interannual to decadal time scales that appears to arise through an off-equatorial trade wind–evaporation–surface temperature feedback and cloud shortwave radiative effects in the central Pacific. When dynamically coupled to the ocean (in fully coupled ocean–atmosphere GCMs), the main change to this mode is increased interannual variability in the eastern equatorial Pacific sea surface temperature and teleconnections in the North Pacific and equatorial Atlantic, though not all coupled GCMs simulate this effect.

Despite the oversimplification due to the lack of interactive ocean dynamics, the physical mechanisms leading to the TCW should be active in the actual climate system. Moreover, the robustness and realism of the spatial patterns of this mode suggest that the physics of the TCW can explain some of the primary features of observed interannual and decadal variability in the Pacific and the associated global teleconnections.

1. Introduction

Sir Gilbert Walker's work in the 1920s and 1930s revealed large-scale correlations in atmospheric surface pressure throughout the tropics and subtropics. He referred to a particular pattern in sea level pressure (SLP) changes as the Southern Oscillation (SO) by which ''is implied the tendency of pressure at stations in the Pacific. . .and of rainfall in India and Java. . .to increase, while pressure in the region of the Indian Ocean decreases'' (Walker 1924). SLP in these regions is linked through the large-scale atmospheric circulation over the tropical Pacific Ocean, the so-called Walker circulation, with mean subsidence over the eastern basin and mean ascent over the western basin. Troupe (1965) wrote about the SO, confirming the patterns observed by Walker, but also noting that the periodicities and persistence of the SO varied with time. Subsequent studies by Bjerknes (1969), Wyrtki (1975), and others revealed that, on interannual time scales, variability in SO is strongly correlated with changes in the thermal structure of the ocean associated with El Niño. Decades of observational, theoretical, and numerical modeling research has now shown

Corresponding author address: Amy Clement, Rosenstiel School of Marine and Atmospheric Science, University of Miami, 4600 Rickenbacker Cswy., Miami, FL 33149.
E-mail: aclement@rsmas.miami.edu

DOI: 10.1175/2011JCLI3973.1

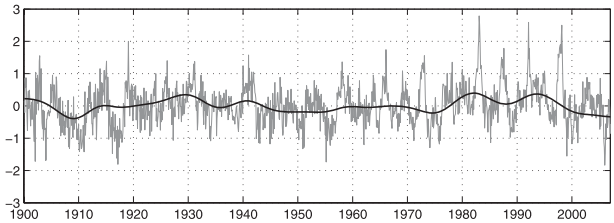

FIG. 1. Monthly SO index [sea level pressure (mb) in 5°S–5°N, 100°W–180° minus 5°S–5°N, 90°–140°E) from the Hadley Centre SLP (HadSLP) reconstruction (Rayner et al. 2003)]. The black curve shows the low-pass-filtered SO index (computed using a Butterworth filter with a 10-yr cutoff period).

that this is the result of dynamical coupling between the ocean and atmosphere, which results in the growth of perturbations to the tropical Pacific climate on seasonal to interannual time scales, generally referred to as the Bjerknes feedback. Hence, the SO is generally thought of as being part of a coupled phenomenon known as the El Niño–Southern Oscillation (ENSO).

A time series of the SO, however, shows variability on longer-than-interannual time scales as well (Fig. 1). Decadal time-scale variability in the SO has been widely noted in the literature, and has been shown to be associated with climate and ecosystem changes throughout the Pacific basin (Mantua et al. 1997; Minobe 1997; Zhang et al. 1997; Hare and Mantua 2000; Peterson and Schwing 2003; Deser et al. 2004, 2006, among others) and extending to the North American hydroclimate (Schubert et al. 2004; Seager et al. 2005). There is also a longer time-scale trend toward a weakening Walker circulation, reflected in the SLP, over the twentieth century (Vecchi et al. 2006; Deser et al. 2010a), which has been attributed to greenhouse gas forcing (Vecchi et al. 2006). The spatial patterns of SLP and sea surface temperature (SST) change associated with changes in the SO are similar on interannual and decadal time scales, though their magnitudes differ (Fig. 2) (Zhang et al. 1997). Are the mechanisms of SO variability on these time scales similar as well?

There is a large body of work that deals with this question by examining the mechanisms that can produce ''ENSO like'' variability on decadal time scales. Here, we adopt the terminology ENSO-like, which is often used in the literature to describe warming in the eastern equatorial Pacific on longer than interannual time scales. The ENSO-like SST pattern associated with the SO that occurs on decadal and longer time scales is not identical to El Niño events, which have their largest signals along the equator, but is otherwise largely similar (Figs. 2c and 2d). (The spatial correlations between the high- and low-pass patterns shown in Fig. 2 in both SST and SLP are 0.9 or greater.) Analogous to the interannual time scale, the mechanisms of decadal ENSO-like variability that have been proposed generally involve a fundamental role for ocean dynamics. These mechanisms include gyre circulation in the North Pacific Ocean (e.g., Latif and Barnett 1994; Barnett et al. 1999; Pierce et al. 2000, 2001), tropical–extratropical ocean exchange (e.g., Gu and Philander 1997), basin-scale oceanic modes (e.g., Yeh and Kirtman 2006), and internal tropical ocean–atmosphere dynamics (e.g., Zebiak and Cane 1987; Karspeck and Cane 2002). Some studies have argued that decadal ENSO-like variability is simply the rectified effect of asymmetry between El Niño and La Niña events (Newman et al. 2003; Rodgers et al. 2004; Vimont 2005; van Oldenburg et al. 2005; An et al. 2007; Philip and van Oldenborgh 2009), so that decades with more El Niño events than La Niña events will look ENSO like.

There are, on the other hand, a smaller number of studies that challenge the notion that interactive ocean dynamics are required for ENSO-like climate anomalies to develop in the Pacific on interannual to decadal time scales. Zhou and Carton (1998) argued on the basis of a simple model that a westward-propagating equatorial SST mode can arise without interactive ocean dynamics through a nonlocal wind–evaporation–SST feedback. Hameed et al. (1989) and Kitoh et al. (1999) showed that in an atmospheric GCM coupled to a mixed layer ocean model (i.e., no interactive ocean dynamics) ENSO-like SST anomalies develop on an interannual time scale. Kitoh et al. argued that a shortwave cloud feedback in the eastern equatorial Pacific is responsible for the SST fluctuations in the model. Chang et al. (2007) have argued that ENSO-like variability can be forced from the North Pacific via an interaction between the atmosphere and surface ocean, again without coupled ocean dynamics. This interaction involves variability in the NE trades, which alters the north–south SST gradient and leads to a meridional displacement in the ITCZ (i.e., the so-called meridional mode; see Vimont et al. (2003) and Chiang and Vimont (2004). Chang et al. (2007) performed experiments with an ACGM coupled to an ocean mixed layer, and showed that ENSO-like SST anomalies can be driven by this meridional mode without a contribution from interactive ocean dynamics. Dommenget (2010) used an AGCM coupled to a static ocean to show that tropical Pacific anomalies develop on an interannual time scale through atmospheric processes, a so-called slab-ocean El Niño. These slab-ocean El Niño events propagate westward via feedbacks between cloud shortwave forcing and surface winds, similar to those proposed by Zhou and Carton (1998), but with an additional cloud–shortwave feedback. Dommenget

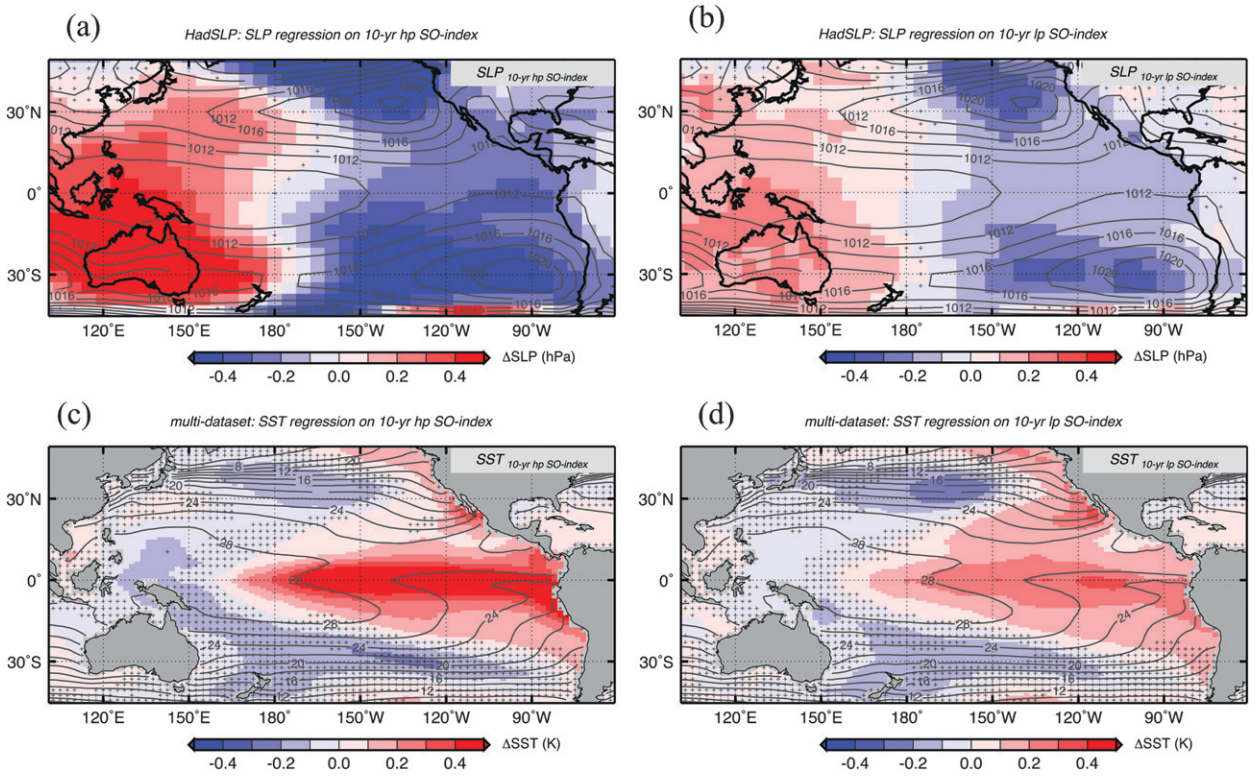

FIG. 2. Regression of observed SLP on monthly observed (a) high- and (b) low-pass-filtered (Butterworth filter, 10-yr cutoff) SO index, using the HadSLP reconstruction version 2 (HadSLP2; Allen and Ansell 2006). Stippling in (a) and (b) indicates areas that are not significant at the 1-σ level (67%) based on a t test with reduced degrees of freedom (DOFs) to account for the autocorrelation in the filtered SO index. Multidataset ensemble-mean regression of SST on monthly observed (c) high- and (d) low-pass-filtered (Butterworth filter, 10-yr cutoff) SO index. Three datasets are used here: the Hadley Centre Sea Ice and Sea Surface Temperature dataset (HadISST; Rayner et al. 2003), and versions 2 and 3 of Smith et al.'s (2008) extended reconstruction SST dataset (ERSSTv2 and ERSSTv3). We chose to average the three datasets in order to emphasize the patterns that are present in all datasets, but overall the patterns do not change significantly from dataset to dataset. Stippling in (c) and (d) indicates areas that are not robust, which is defined as being where 1) the datasets do not agree in sign and 2) where the regression values are not significant at the 1-σ level (67%) based on a t test with reduced DOFs to account for the autocorrelation in the filtered SO index. All regressions are performed on the normalized SO, so units are hPa (for SLP) and K (for SST). All data are detrended and regressions are computed for the 1880–2004 period. Similar patterns appear in nonreconstructed datasets as well (see, e.g., Zhang et al. 1997).

and Latif (2008) used a similar model configuration but with ocean mixing down to 500 m included, which shows that ENSO-like variability can arise on time scales up to millennia. In that model, they argued, the SST variability is driven by latent heat flux anomalies, and their analysis suggests that the "source" is variability in the North Pacific atmospheric circulation, which is transmitted to the tropics via atmospheric teleconnections.

There is no doubt that El Niño and the Southern Oscillation are linked by both thermodynamic and dynamic coupling between the ocean and atmosphere. But how fundamental is this linkage? Can one exist without the other? Here, we address these questions by examining the temporal and spatial characteristics of tropical Pacific atmospheric variability with varying degrees of coupling to the ocean.

2. Model experiments

We use a set of experiments with the Community Atmosphere Model (CAM) version 3, which was developed at the National Center for Atmospheric Research (NCAR) (Collins et al. 2006b). The first experiment is one in which CAM is forced by climatologically varying SSTs. In this integration, SSTs and sea ice are prescribed to vary with a repeating seasonal cycle, but there is no year-to-year variability. The SST and sea-ice conditions are based on observations during the period 1980–2000 from the dataset of Hurrell et al. (2008), and CAM3 is coupled to the Community Land Model (CLM; Oleson et al. 2004). Five hundred years of this simulation are analyzed here; further analysis is presented in Deser et al. (2010b). This represents the case in which the atmosphere

TABLE 1. Statistics of the SO index [SLP in the western Pacific (5°S–5°N, 100°E–180°) minus the eastern equatorial Pacific (5°S–5°N, 170°E–140°W)], and Niño-3 index (monthly SST anomaly averaged over 5°S–5°N, 170°E–140°W), from observations, AGCM-slab models, and fully coupled models. The lengths of the slab simulations for each model are highly variable and are provided in the first column. For all of the coupled models, 500 yr of the simulation time are used. The decorrelation time scale is defined here as the *e*-folding time scale of the autocorrelation function of the Niño-3 index.

Model	Length of slab simulation	Std dev SO slab (Pa)	Std dev SO coupled (Pa)	Std dev Niño-3 slab (K)	Std dev Niño-3 coupled (K)	Decorrelation time scale in coupled models	Decorrelation time scale in slab models
Obs	—	—	80	—	0.80	7	—
CCCma	30	42	61	0.24	0.44	5	5
CCCma T63	30	43	60	0.25	0.40	6	9
CSIRO	60	54	74	0.20	0.92	6	15
GFDL CM2.0	50	51	89	0.22	0.85	6	9
GFDL CM2.1	100	61	135	0.3	1.3	7	10
GISS	120	34	46	0.13	0.22	8	7
INM-CM3	60	31	50	0.25	0.86	6	16
MIROC(hires)	20	39	45	0.41	0.34	6	13
MIROS(medres)	60	46	49	0.33	0.46	10	17
MPI ECHAM5	100	72	113	0.3	1.23	8	11
MRI	150	55	84	0.33	0.68	5	28
NCAR CCSM3	200	39	73	0.30	0.80	6	13
HadGEM1	70	64	75	0.49	0.64	6	13
Multimodel mean	—	49	73	0.29	0.70	6.5	13

and ocean are essentially uncoupled, and will be referred to as CAM-climo. In the second experiment, CAM is coupled to a 50-m slab ocean, referred to as CAM-slab. An additional ''*q* flux'' term is added to the SST equation of the slab ocean to represent the effects of ocean heat transports on the mean observed climate, but this term does not vary with time. Hence, in this case, the atmosphere is thermodynamically coupled to the ocean through heat and moisture fluxes but is not dynamically coupled. The third experiment is the one in which CAM is coupled to a full-ocean GCM, the Community Climate System Model (CCSM3; Collins et al. 2006a). All experiments are performed at T85 (approximately 1.4°) resolution in the atmosphere, but simulations with other resolutions (T42 and T31) have been analyzed and the main findings are not sensitive to the model resolution.

We also use a collection of control simulations made available through the Program for Climate Model Diagnosis and Intercomparison (PCMDI). We use 13 models, each of which has a version in which the atmospheric GCM is coupled to a 50-m-slab mixed layer ocean (as in the CAM-slab simulation, referred to hereafter as AGCM-slab models), and a fully coupled version. The following models are used: the Canadian Centre for Climate Modelling and Analysis (CCCma), CCCma T63, Commonwealth Scientific and Industrial Research Organisation (CSIRO), Geophysical Fluid Dynamics Laboratory Climate Model versions 2.0 and 2.1 (GFDL CM2.0 and GFDL CM2.1), Goddard Institute for Space Studies (GISS) Model E, Hadley Centre Global Environmental Model version 1 (HadGEM1), Institute of Numerical Mathematics Coupled Model, version 3.0 (INM-CM3), the medium- and high-resolution versions of the Model for Interdisciplinary Research on Climate 3.2 [MIROC(hires) and MIROC(medres)], Max Planck Institute (MPI) ECHAM5, Meteorological Research Institute (MRI), and NCAR Community Climate System Model, version 3 (CCSM3). The lengths of simulations in the AGCM-slab models vary (Table 1), and we use 500 yr of the fully coupled model simulations for the analysis performed here.

3. Results

a. CAM experiments

An EOF analysis of normalized monthly sea level pressure anomalies (relative to a fixed annual cycle) was performed on all three CAM configurations, and results are shown in Fig. 3. The dominant mode of variability in CAM-climo is a zonally symmetric structure explaining 72% of the variance. EOF analysis performed on global fields (not shown) reveals that tropical changes are out of phase with SLP at high latitudes, and this mode therefore represents a shift of atmospheric mass between the low and high latitudes. This mode is uncoupled to the ocean, so while it appears in CAM-slab and CCSM, it explains less of the SLP variability in those simulations (55% in CAM-slab and 48% in CCSM) and is not associated with any pattern of SST variability. If we remove this mode from CAM-slab and CCSM (by

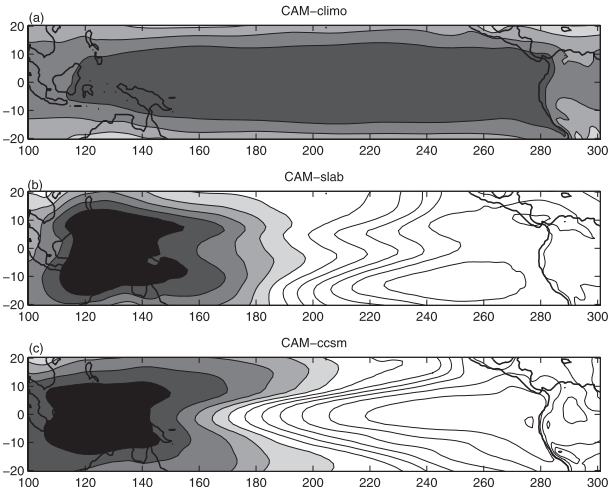

FIG. 3. The leading EOFs of monthly normalized (to unit standard deviation) SLP anomalies in (a) CAM-climo, (b) CAM-slab, and (c) CCSM; the variances explained by the mode shown are 72%, 28%, and 50% , respectively. The pattern in (a) was removed from CAM-slab and CCSM before computing the EOFs. See text for details. Negative values are shaded. The contour interval is the same in all panels.

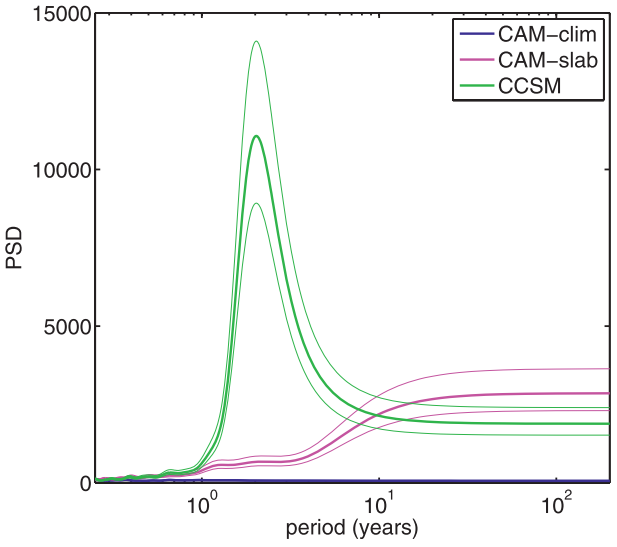

FIG. 4. Spectra of the monthly SO index in CAM-climo (blue), CAM-slab (pink), and CCSM (green). The 95% confidence intervals on the spectra are shown.

linearly regressing the SLP field onto this pattern and subtracting it from the total field), the dominant mode of the SLP variability in CAM-slab now resembles the SO (Fig. 3b) and explains 28% of the monthly SLP variability. The dominant mode in CCSM is also the SO, but with enhanced amplitude on the equator relative to CAM-slab. It also explains more variance (50%) than in CAM-slab. In CCSM, this mode represents the model's simulation of ENSO.

The spectral properties of the SO index in the three model configurations are shown in Fig. 4. (The results are the same if we instead use the principal component of EOF1 in CAM-slab and CCSM.) The SO index in CAM-climo has very little power [standard deviation is 20 Pa; for reference, the standard deviation of the observed SO index (shown in Fig. 1) is 80 Pa] and a white spectrum. When the atmosphere is thermodynamically coupled to the ocean (CAM-slab), the standard deviation of the SO doubles and the spectrum of the SO becomes red. This spectrum is consistent with the integration of atmospheric white noise by the mixed layer ocean (as in Frankignoul and Hasselmann 1977), and in this model there is a decorrelation time scale of the Niño-3 index (defined as the *e*-folding of the autocorrelation function) of 13 months. The addition of interactive ocean dynamics in CCSM increases the power in the SO index (standard deviation is about 70 Pa, still somewhat smaller than the observations; see Table 1), but primarily in the interannual band (Fig. 4). The decorrelation time scale is also shortened to 6 months with the addition of interactive ocean dynamics (Table 1), which is consistent with the interpretation of the spectra that coupled ocean dynamics enhance variability on seasonal to interannual time scales (via the Bjerknes feedback), but that on longer time scales dynamical oceanic adjustments provide a slow restoring force to the unstable equatorial air–sea interactions [i.e., as described in reviews by Neelin et al. (1998) and Chang et al. (2006)]. This quasi-biennial spectral peak represents the ENSO simulation in CCSM, as previously reported (Deser et al. 2006). At decadal and longer time scales, the addition of coupled ocean dynamics reduces the variance in the SO relative to CAM-slab.

b. Multimodel analysis of the thermally coupled Walker mode

We refer to the mode of variability that emerges from the CAM-slab, which has a spatial structure like that of the Southern Oscillation and a power spectrum consistent with a stochastically forced, damped process, as the thermally coupled Walker mode (TCW). We use this terminology to make the distinction from the real-world Walker circulation (the surface manifestation of which is the SO), which is fully coupled to the ocean, since the TCW is only coupled to the ocean through heat and moisture flux at the ocean surface. Here, we examine the temporal and spatial characteristics of the TCW in a multimodel context.

Figure 5 shows the spectra of the SO index in the AGCM-slab ocean models. All models show spectral properties similar to those of CAM-slab (Fig. 4). Results are similar for the Niño-3 index (not shown), which can more easily be interpreted physically within

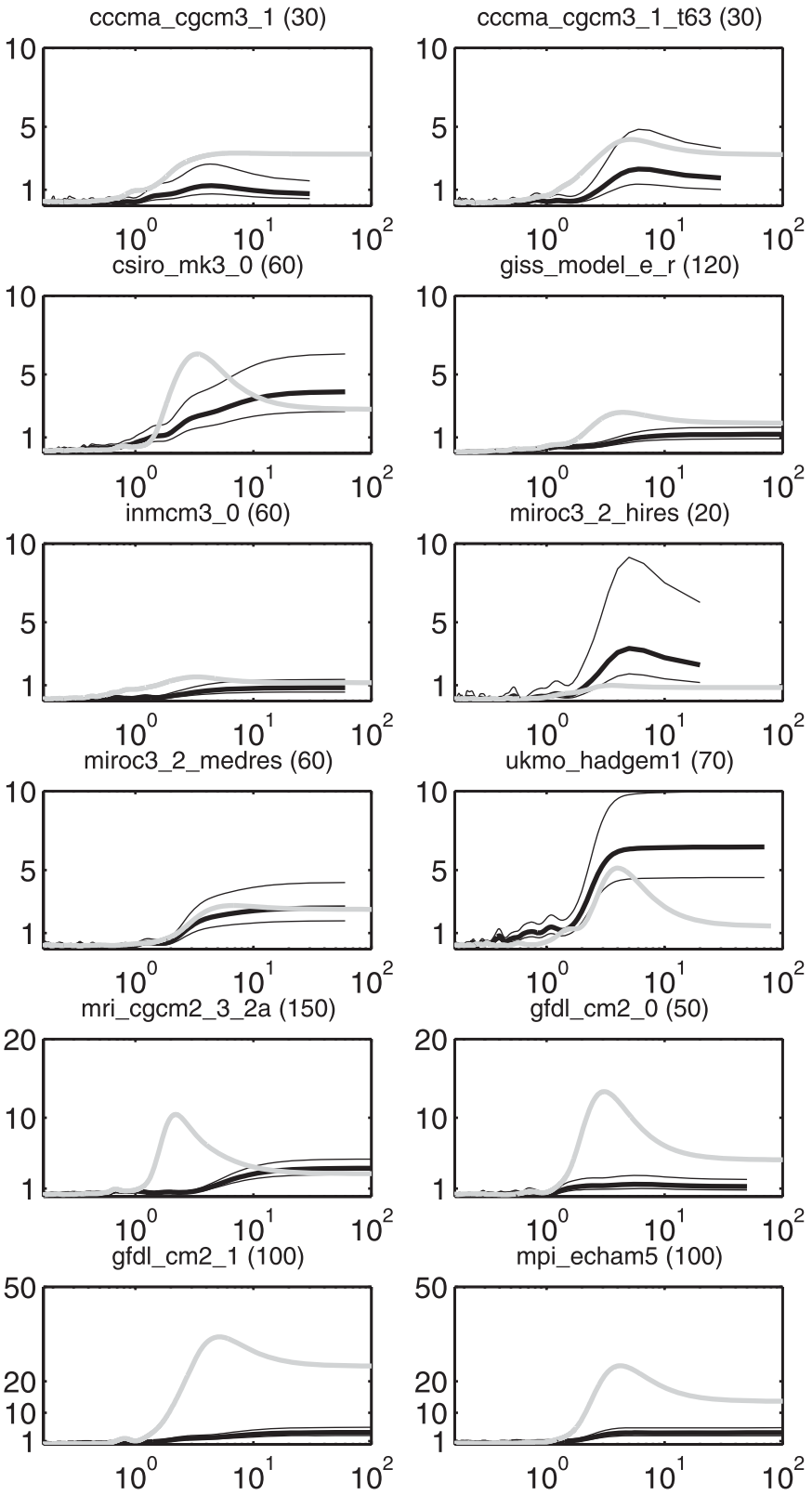

FIG. 5. Spectra of the SO index for individual models. Black lines are from the slab versions of the model (with 95% confidence intervals shown in light gray lines) and gray lines are from the coupled versions. The x axis shows the period (yr). Each slab simulation is a different length (numbers of years are indicated at the top of each panel, and also in Table 1), but for all coupled models we use 500 yr of the control simulation.

the Frankignoul and Hasselmann (1977) context, with ''damping'' arising from surface fluxes. A fit of the model to the multimodel mean spectrum of Niño-3 yields a damping rate of 6 W m^{-2} K^{-1}, which for a 50-m mixed layer translates into a characteristic damping time scale of about 15 months. This damping rate is low compared to the range of values computed for observations (Park et al. 2005), suggesting that this process is weakly damped. It has been suggested such low damping rates can be expected on longer than seasonal time scales if longwave cooling is the dominant damping process (Barsugli and Battisti 1998; Du and Xie 2008). The decorrelation time varies from model to model (Table 1), which is not surprising since this involves numerous processes, including clouds (Park et al. 2005), which are highly model dependent. Of particular note is the MRI model, which has an extremely long decorrelation time scale (greater than 2 yr), and which is consistent with the Kitoh et al. (1999) analysis of an earlier version of that model showing a positive feedback (weaker damping) involving clouds in the tropical Pacific. However, Lloyd et al. (2010) have shown that in Atmospheric Model Intercomparison Project (AMIP) mode the cloud feedbacks were problematic in this model.

Despite the absence of interactive ocean dynamics in the AGCM-slab simulations, the patterns of climate variability associated with the TCW are remarkably realistic. The global regression of SLP and precipitation anomalies on the SO index in the AGCM-slab models (Figs. 6c and 6d) have patterns and amplitudes showing striking similarity with observations (Figs. 6a and 6b). All regressions shown in this paper are based on normalized indices, so they represent a response per unit standard deviation change in the index. The larger magnitude of the SLP regressions in the observations therefore indicates that other feedbacks (not simulated in the AGCM-slab model) amplify the response. The AGCM-slab SLP pattern, however, has all of the features of the SO originally observed by Walker (1924) [and reconfirmed more recently by Trenberth and Caron (2000)], with out-of-phase changes in the Eastern and Western Hemispheres (separated by the date line), and also a large signal in the Amundsen–Bellingshausen Sea, which Van Loon and Shea (1985) argued was actually a precursor to changes in the SO. There is also a connection to the North Pacific, but the signal simulated in the AGCM-slab simulation in that region is weaker and does not extend into the subtropics as in the observations. The precipitation patterns in the tropical Pacific are consistent with the observed patterns, which occur on interannual and decadal time scales as noted by Deser et al. (2004), particularly in the South Pacific convergence zone (SPCZ). The observed precipitation change over North America that has been linked with climate changes in the tropical Pacific—warmer tropical Pacific, more precipitation over North America (Schubert et al. 2004; Seager et al. 2005)—is also simulated in association with the TCW. The AGCM-slab models do not simulate the signal in the tropical Atlantic–northeastern Brazil region, which is an area of known ENSO teleconnections on interannual time scales (e.g., Hastenrath and Heller 1977).

Additional patterns of climate changes in the Pacific basin associated with the SO in the AGCM-slab models are shown in Fig. 7. The simulated SST shows an ENSO-like pattern of warming (Fig. 7a) associated with the SO that agrees with the observations, particularly on decadal time scales where both the magnitude and pattern are in agreement (Fig. 2b). This coincides with an eastward shift of convection, reflected in the midtropospheric vertical velocity (Fig. 7b), an increase in cloud cover over the central Pacific (Fig. 7d), and a weakening of the equatorial trade winds in the central Pacific (Fig. 7c) (i.e., a weakening of the Walker circulation).

One difference between the simulated patterns associated with the TCW and the observed 10-yr low-pass-filtered patterns in the Pacific (Fig. 2) is that the observations show a maximum SST signal on decadal time scales in the northeastern Pacific that is absent in the models. Clement et al. (2009) have argued that this observed decadal signal in the northeastern Pacific is related to changes in stratus cloud cover. Those authors also pointed out that models, in general, fail to simulate the observed relationships between cloud and regional meteorology in that region, and accordingly there is no robust change in clouds in the eastern Pacific (Fig. 7d). This suggests that the absence of the SST signal in the NE Pacific in the models could be in part explained by a poor simulation of low-level cloud variability in that region.

c. *The TCW mechanism*

The ENSO-like SST warming pattern comes about primarily from weaker northeast and southeast trade winds. To illustrate this, we show the regressions of various fields onto the 2-yr low-pass-filtered tendency of the SO ($d\mathrm{SO}/dt$). The regressions indicate what this mode looks like as it is developing. We use a 2-yr low-pass filter to emphasize the effects of mixed layer integration.

Figure 8a shows that the integrated heating associated with the developing SO indeed looks like the pattern of the SST anomaly associated with SO (Fig. 7a), and the magnitude of the net heat flux (maximum of about 4 W m^{-2}) is consistent with a warming of 0.2 K for a 50-m mixed layer on a seasonal time scale. This warming pattern

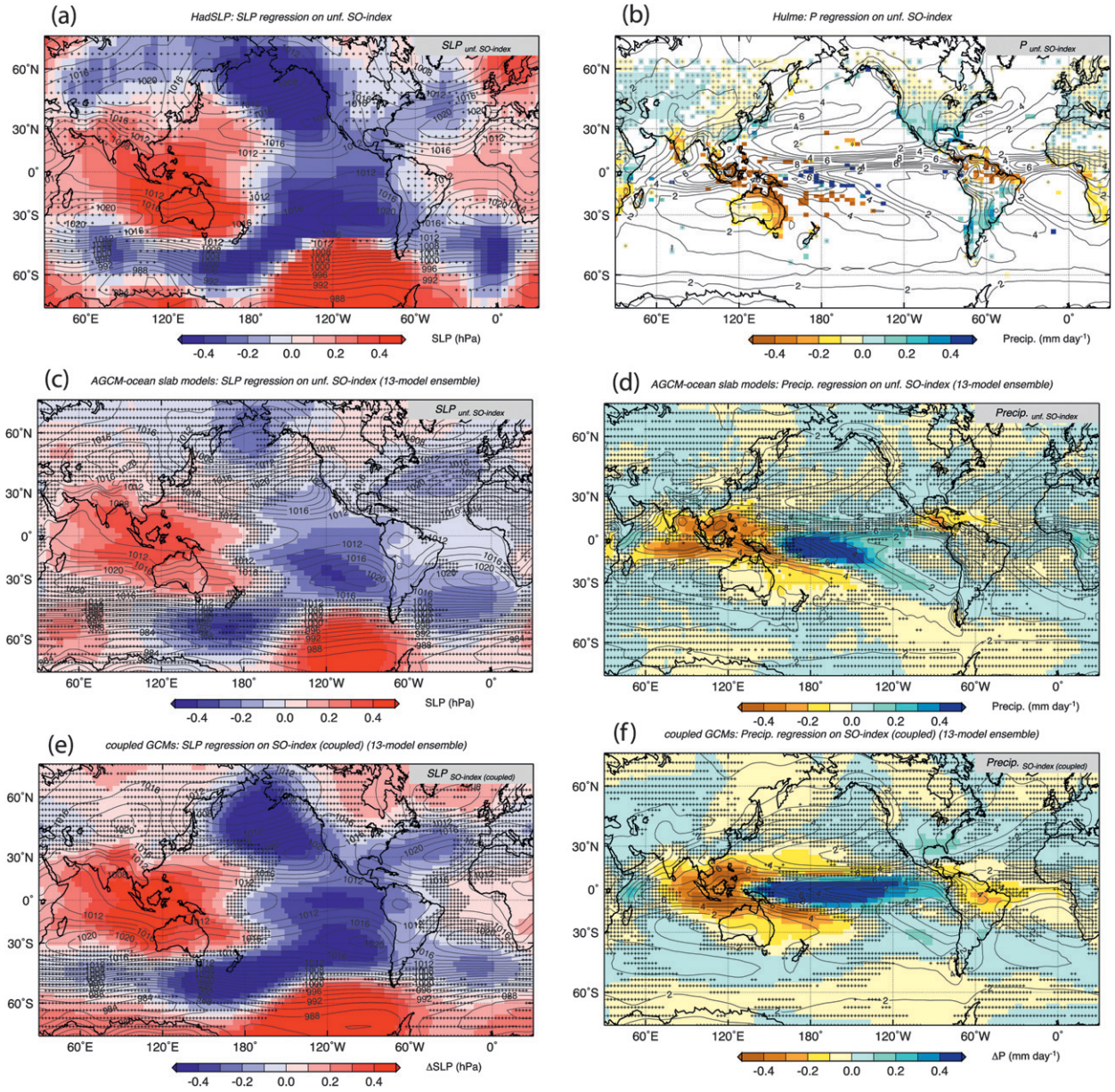

FIG. 6. Observed regression of global (a) SLP and (b) precipitation on the normalized SO index. The observed SLP data are from HadSLP2 (Allen and Ansell 2006) and the precipitation is from land stations (Hulme et al. 1998). Stippling indicates areas where the signal is not significant at a 1-σ level (67%) based on a t test with reduced DOFs to account for the autocorrelation in the filtered SO index. In Fig. 6b, the contours are the 1979–2003 annual-mean climatology from the Global Precipitation Climatology Project (GCPC) version 2 analysis (Adler et al. 2003). Multimodel ensemble-mean (c) SLP and (d) precipitation regressions on the (normalized) SO indexes of 13 AGCM-slab models. Multimodel ensemble-mean (e) SLP and (f) precipitation regressions on the (normalized) SO indexes of 13 fully coupled models. In Figs. 6c–f, stippling shows where the multimodel changes are *not* robust. A multimodel change is considered robust when more than 10 models (out of 13) have the same sign as the multimodel mean. Multimodel ensemble-mean climatological annual-mean fields from the observational and multimodel datasets are shown in black contours.

mainly comes from the latent heat flux (Fig. 8b), which is shown as positive into the ocean (red colors indicate ocean warming by reduced latent heat flux). The reduced latent heat flux coincides with a weakening of the trade winds (Fig. 8c), which is consistent with a wind-induced latent heat flux change since there is little SST signal in those regions (Fig. 8e). The off-equatorial cooling in the west is also consistent with the altered circulation. Southerly advection warms the western basins (Seager et al. 2003), so weaker advection

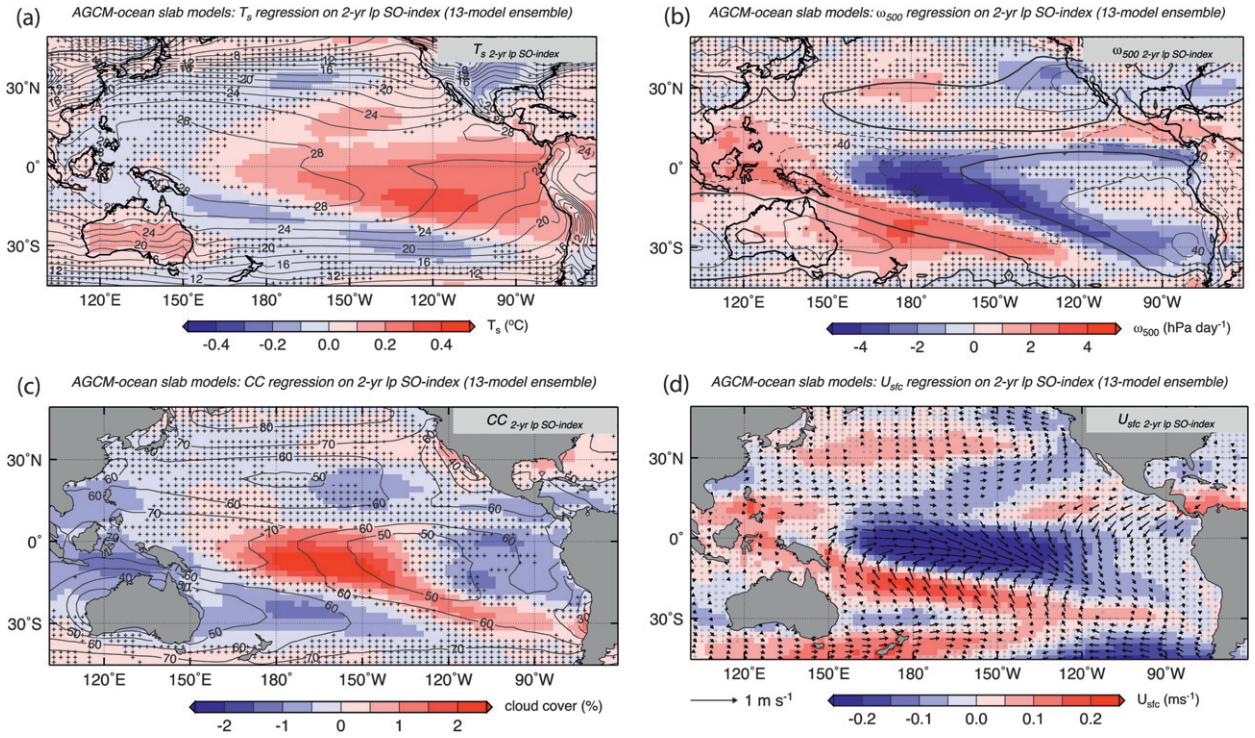

FIG. 7. AGCM-slab multimodel means from 13 models of (a) SST, (b) omega 500 hPa, (c) total cloud cover and (d) wind vectors and speed regression on the (normalized) SO index. Stippling shows where the multimodel changes are *not* robust. A multimodel change is considered robust when more than 10 models (out of 13) have the same sign as the multimodel mean. Contours show the multimodel annual-mean climatology of each variable.

is consistent with cooling. There is also an increase in the westerlies, which would lead to cooling by increased latent heat flux (Hazeleger et al. 2001). [We note that a change in wind speed is not well captured using monthly mean wind components, since in the subtropics and midlatitudes, mean wind speed is dominated by transient eddies. However, submonthly data for calculating the wind speed are not available for many of these simulations.] As this mode is developing, there is little temperature change in much of the tropical Pacific (Fig. 8e). There is a small warming in the eastern subtropics where the trade winds are reduced, consistent with the reduced latent heat fluxes, particularly in the Southern Hemisphere.

Is there an important role for cloud feedbacks in this mode, or does it grow only through surface latent heat flux? The latent heat flux alone (Fig. 8b) would not produce warming in the central Pacific around the date line, which is present in the fully developed SO-related SST pattern (Fig. 7a). Figure 8d shows that there is a robust cloud radiative heating pattern in the central equatorial Pacific, which is due to a reduction in cloud cover there. Our interpretation of this change in cloud cover is that it is also tied to the reduction in the trade winds, which reduces the mass flux convergence in the lower atmosphere, as indicated by the vector winds in Fig. 8d. That central Pacific cloud-driven warming, though small, may contribute to the eastward shift of convection, leading to the fully developed cloud change pattern shown in Fig. 7d. It is unclear from these experiments whether the cloud signal in the central Pacific is required to shift the convection eastward and weaken the Walker circulation. Further experiments are necessary to test that idea.

This analysis suggests that weakening of the northeast and southeast Pacific trade winds lowers the ocean-to-atmosphere latent heat flux in the eastern basin and reduces cloud cover in the central Pacific due to diminished low-level convergence, which leads to an ENSO-like eastern Pacific warming, an eastward shift in convection, and a weakening of the Walker circulation. What is the origin of the trade wind variability? Vimont et al. (2003) have suggested that North Pacific variability can influence the tropical climate via a feedback between the trade wind variability and the north–south SST gradient, which leads to a meridional displacement in the ITCZ and in turn influences the SST gradient. This interaction has been described as a meridional mode (Vimont et al. 2003; Chiang and Vimont 2004). On the other hand, Terray (2010) has shown using observations that a similar meridional mode operates in the South Pacific, Indian, and Atlantic basins and influences observed ENSO

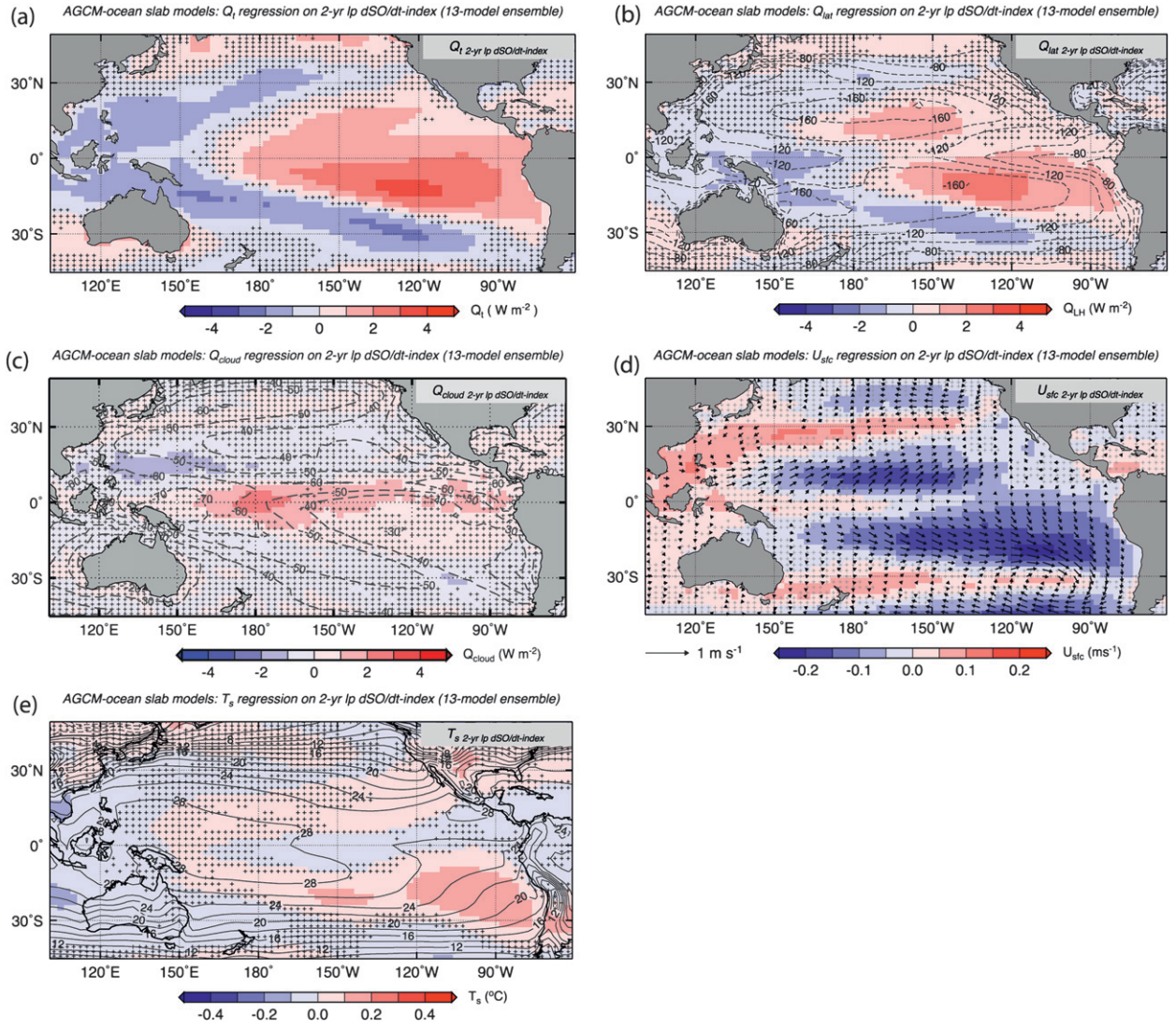

FIG. 8. (a) AGCM-slab mixed layer heat content tendency (W m^{-2}; equivalent to the net surface heating in the AGCM-slab configuration) regressed on the time derivative of the Southern Oscillation index. The fields are low-pass filtered with a 2-yr cutoff (though the exact cutoff does not affect the results). (b) As in (a), but for latent heat flux (W m^{-2}). (c) As in (a), but for net cloud radiative forcing (W m^{-2}). (d) As in (a) but for surface wind vectors and speed (m s^{-1}) computed using the monthly mean data. (e) As in (a), but for surface temperature (°C). All surface fluxes are defined as positive into the surface. Stippling shows where the multimodel changes are *not* robust. A multimodel change is considered robust when more than 10 models (out of 13) have the same sign as the multimodel mean. Contours show the multimodel ensemble-mean annual-mean climatology of each variable.

variability. Interestingly, all models show a distinct seasonality to the TCW that is remarkably consistent with the observed SO (Fig. 9). The observed seasonality, with maximum variability in the boreal winter, has been interpreted by Vimont et al. (2003) and Chang et al. (2007) to suggest that boreal spring trade wind variability is responsible for the development of climate anomalies 9 months later (during boreal winter) via coupled feedbacks. However, our results suggest that both Northern and Southern Hemisphere trade winds contribute to the development of the TCW, and it is as yet unclear whether the TCW seasonality comes from the Northern or Southern Hemisphere.

d. The role of interactive ocean dynamics

In the real world, of course, the ocean and atmosphere are coupled both dynamically and thermodynamically. How does dynamical coupling with the ocean affect the spatial and temporal features of the SO? To address this question, we perform the analyses of the previous section on the fully coupled versions of the 13 models. In all of the models, the addition of coupled ocean dynamics

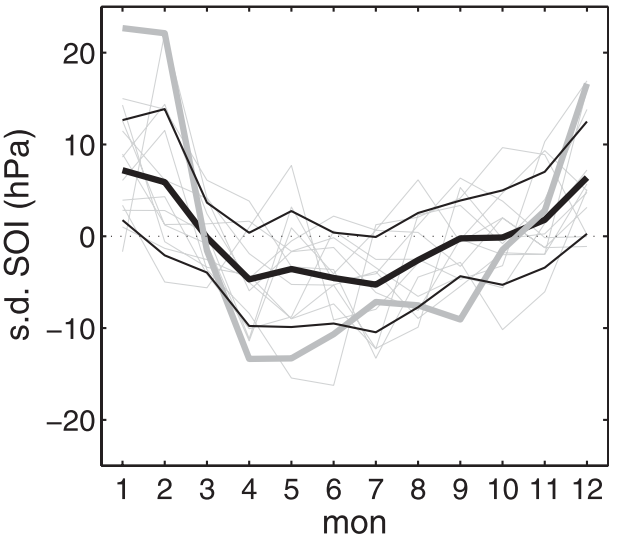

FIG. 9. Seasonality of the standard deviation of the SOI in the slab-ocean AGCM models (thin gray lines) and observations (thick gray line). The mean standard deviation for all months is removed from each individual model in order to emphasize the seasonality. The multimodel mean and 1-σ envelope are shown by the black lines. Observations correspond to the HadSLP analysis. The climatological monthly mean seasonal cycle is removed from the SOI before computing the standard deviation for each calendar month.

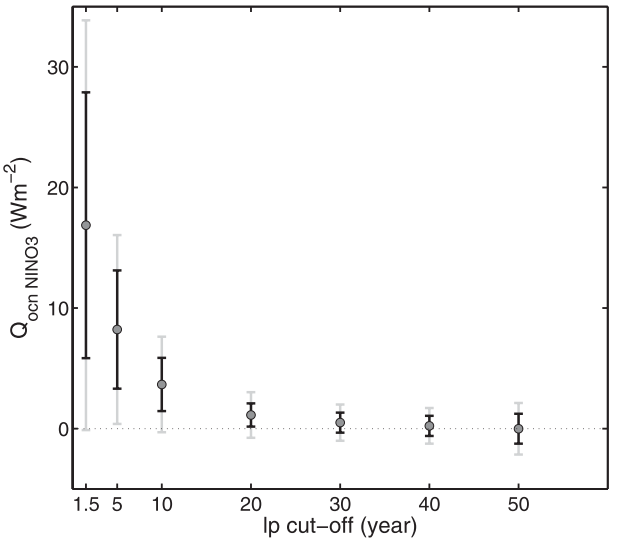

FIG. 10. The ocean dynamical contribution to the growth of the SO in the Niño-3 region. The ocean dynamical heating Q_{ocn} is calculated by taking the difference between the net surface heating (Qnet) and the ocean mixed layer temperature tendency ($\rho c_p H \partial T/\partial t$) with $H = 100$ m. The values plotted along the y axis are the regression of ocean dynamical heating on the low-pass-filtered time tendency of the SO index (dSO/dt) for several of the cutoff frequencies. The gray error bars are the maximum–minimum range among the 11 models that have made ocean data available in the CMIP3 archive. The black error bars are the 1-std dev range.

increases the standard deviation of the SO about 50%, and Niño-3 by 130% (Table 1). This occurs predominantly in the interannual band (Fig. 5). In some coupled models (e.g., the GFDL models, MPI, MRI, CCSM, and CSIRO), interactive ocean dynamics produce the expected effect of the Bjerknes feedback, namely that perturbations to the tropical Pacific climate will grow on seasonal-to-interannual time scales through a feedback between the SST, trade winds, and thermocline tilt. Ocean dynamics are, in principle, also responsible for the termination of El Niño events via either the delayed oscillator mechanism or the recharge–discharge mechanism (Jin 1997; Neelin et al. 1998), and the result is an interannual spectral peak that is not present in the AGCM-slab models (Fig. 5). This negative ocean feedback is also consistent with the shorter decorrelation time scale in coupled models compared with AGCM-slab models (Table 1). However, in some models (e.g., CCCma, CCCma T63, and GISS) the addition of interactive ocean dynamics does not introduce a clear spectral peak at interannual time scales, and in other models [e.g., MIROC(medres) and INM-CM3], interactive ocean dynamics does not appear to significantly alter the spectral properties of the SO at all (Fig. 5). In these models, ENSO variability is weak and has been shown to be consistent with an "SST mode" (Neelin 1991; Jin and Neelin 1993; Guilyardi 2006), in which the thermocline fluctuations do not strongly influence the SST.

On decadal and longer time scales, the effects of interactive ocean dynamics are both weaker and model dependent. This is illustrated in Fig. 10, which shows the contribution of coupled ocean dynamics (see figure caption for an explanation of how this is computed) to the growth of the Niño-3 index on different time scales. On time scales up to about a decade, coupled ocean dynamics, generally speaking, contribute to the net heating that gives rise to SST anomalies in the Niño-3 region. However, it should be noted that not all models simulate this feedback (see gray bars, which indicate the minimum–maximum of this quantity). This is consistent with the spectra (Fig. 5), which show that some fully coupled models do not simulate significantly different power in the SO from the AGCM-slab version on any time scale. Beyond 10 yr, overall, there is little role for ocean dynamics in the Niño-3 region as simulated by these models. There are some models (e.g., GFDL models and MRI) that are known to simulate skewed interannual variability, with larger warm events than cold events, which is consistent with the observations (van Oldenborgh et al. 2005; Philip and van Oldenborgh 2009). This is a mechanism by which those models can produce

decadal time-scale variability as a rectified effect of the interannual variability. Nonetheless, it is clear from Fig. 10 that the ocean does little to amplify the warming in the Niño-3 region on longer than 10-yr time scales.

Why does the positive contribution of coupled ocean dynamics on Niño-3 warming wane at longer time scales? The thermocline tilt and zonal wind stress must balance on all time scales (Clarke 2010), and hence the Bjerknes feedback could be expected to be time-scale independent [e.g., Dijkstra and Neelin (1995) suggested the possibility of a ''climatological Bjerknes feedback'']. However, Cane and Sarachik (1977) and, more recently, Clarke (2010) showed that the quasi-steady adjustment of a shallow-water ocean to equatorial zonal wind stress results in a thermocline change primarily in the western Pacific. Thus, there is a reduced thermocline tilt when the winds are weak, but because it occurs where the thermocline is deep (in the western basin), there is no feedback on the mixed layer temperature. Vecchi et al. (2006) showed that this is consistent with reanalysis data over the last 50 yr.

There are also some models that appear to simulate a negative feedback from coupled ocean dynamics at longer than 10-yr time scales (the gray bars in Fig. 10 extend to negative values). For example, some coupled models [e.g., CCSM, HadGEM1, MIROC(hires)] simulate less power at decadal and longer time scales than their slab counterparts. While we have not identified the specific ocean processes that could produce this effect, a modeling study by Hazeleger et al. (2005) provides some insights into this result. Consider a westerly wind anomaly on the equator that persists on decadal time scales. One can think of this as arising from, for example, the processes that produce the TCW (and yield the wind and associated SST patterns shown in Fig. 7). Hazeleger et al. (2005) performed a set of experiments with uncoupled ocean and atmosphere models, and showed that the poleward ocean heat transport is increased in response to this wind forcing via an increase in the meridional mean overturning in the subtropical ocean cells, which removes the warm equatorial SST anomaly. That is, the ocean circulation response to this wind anomaly is a negative feedback on the wind pattern.

We can also examine whether the spatial features of the SO are altered by interactive ocean dynamics. Figures 6e and 6f show the global SLP and precipitation fields regressed on the SO index from the coupled models. The main features of these patterns are very similar to the corresponding patterns in the AGCM-slab models (Figs. 6c and 6d), although the amplitudes are larger. These larger amplitudes are consistent with the Bjerknes feedback, whereby the ocean contributes to the warming in the eastern equatorial Pacific, giving a bigger response, particularly in the eastern equatorial Pacific, per unit standard deviation change in the SO. The main area of difference in SLP is over the North Pacific, where the coupled models and observations are in quite good agreement, but the AGCM-slab models produce a pattern that is weak and shifted to the north. This suggests a role for ocean dynamics in the variability of the North Pacific climate but it is not clear whether this is a local feedback or results from teleconnections from the tropics (where SST anomalies are larger in the fully coupled case). The main area of difference in precipitation is in the tropical Atlantic, where, again, the fully coupled models and observations are in agreement, while the AGCM-slab model simulates no response. Perhaps this atmospheric teleconnection requires the eastern Pacific precipitation anomalies, which are simulated by the fully coupled models but not by the AGCM-slab models (Saravanan and Chang 2000). Another difference is in the western equatorial Pacific, where the pattern of precipitation anomalies simulated by coupled GCMs is shifted westward compared with the observations and AGCM-slab models, and is likely to result from the cold tongue bias, which is absent in AGCM-slab models that incorporate a prescribed q flux based on observed SSTs.

Interactive ocean dynamics contribute to the SST pattern associated with the SO, but this contribution is time-scale dependent. Figure 11 shows the regression of SST on the high- and low-pass SO results. The SST response is significantly amplified along the equator by coupled ocean dynamics on time scales of less than a decade. However, the longer time-scale variability ($>$10 yr) is in closer agreement with the AGCM-slab models, again supporting the notion that the ocean dynamical effect is confined to shorter than decadal time scales. We note that there appears to be an amplification of the SST signal in the North Pacific on decadal time scales, suggesting that perhaps the gyre time-scale processes are responsible for this signal (Kwon et al. 2010).

We also note that the comparison between the AGCM-slab simulations and the fully coupled simulations is a test of the role of *interactive* ocean dynamics, but the effects of mean ocean dynamics are not tested. In the AGCM-slab simulations, the addition of the q flux results in a warm pool–cold tongue configuration of the tropical Pacific that would be absent without the q flux (Clement et al. 2005). Further experiments are necessary to test how the mean state of the tropical Pacific influences the SO variability.

4. Discussion

This multimodel analysis has shown that Pacific climate anomalies that have an ENSO-like spatial structure

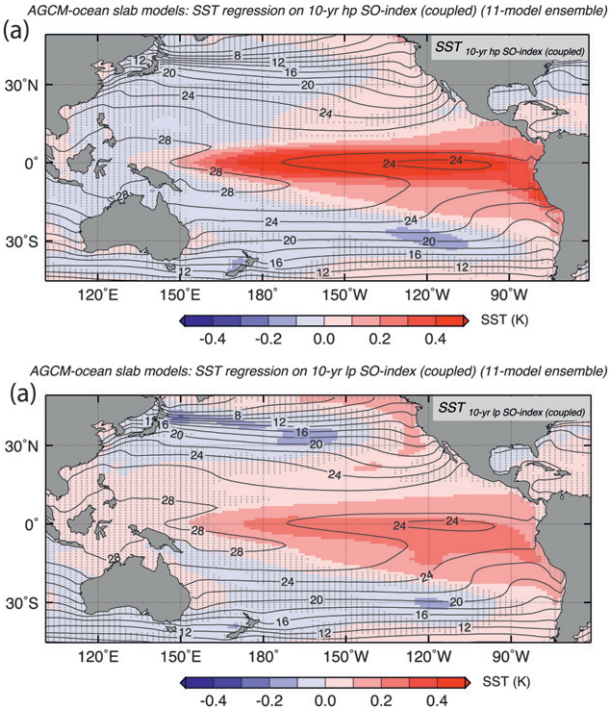

FIG. 11. Multimodel ensemble-mean regression of SST on the normalized (a) 10-yr cutoff high-pass SO and (b) 10-yr cutoff low-pass-filtered SO indexes simulated by coupled GCMs. High- and low-pass time series are normalized, so regressions are shown in kelvins per standard deviation of SO change. Stippling shows where the multimodel changes are *not* robust. A multimodel change is considered robust when more than10 models (out of 13) have the same sign as the multimodel mean. Contours show the multimodel ensemble-mean annual-mean SST climatology.

(warming in the eastern Pacific, eastward shift in convection, weaker Walker circulation) can develop on interannual to decadal time scales without dynamical coupling to the ocean (i.e. with no Bjerknes feedback). Here, we discuss the implications of this result for Pacific climate variability on different time scales.

a. Interannual time scale

It has previously been suggested that observed El Niño events are preceded by a weakening of the NE trade winds in boreal spring (Chang et al. 2007). Chang et al. argue that a meridional mode that links variability in the North Pacific to the deep tropics influences the equatorial wind stress, which can then trigger an event. The meridional mode develops through a wind–evaporation–surface temperature (WES) feedback that does not require dynamical coupling to the ocean. A more recent observational study by Terray (2010) shows that a similar meridional mode also operates in the Southern Hemisphere and can be used to predict El Niño events with some skill. Our results are consistent with this interpretation of the observations from both the Northern and Southern Hemispheres. That is, variability in the trade winds of both hemispheres (with a pattern like that shown in Fig. 8d) influences the net surface heating, yielding an SST pattern that has an ENSO-like structure that develops on interannual time scales. This interpretation is also consistent with an earlier observational analysis of Penland and Sardeshmukh (1995), who showed that the optimal surface temperature pattern that gives rise to El Niño events 7 months later (their Fig. 6) looks very much like the pattern shown in Fig. 8e (i.e., the "developing" pattern of SST). [Yeh and Kirtman (2006) also show this for a coupled GCM.] We interpret this temperature signal in the multimodel analysis as being the surface expression of the trade wind variability shown in Fig. 7d [i.e., the same temperature change that occurs within a short (<2 yr) time in response to a wind-driven change in latent heat flux]. This interpretation of the Penland and Sardeshmukh (1995) pattern also provides a mechanism by which the off-equatorial SST pattern can be related to changes along the equator, since there is an equatorial mass flux divergence associated with the trade winds (Fig. 8d). There is no doubt that coupled ocean dynamics can amplify an ENSO-like perturbation on interannual time scales via the Bjerknes feedback. However, these results suggest that the development of ENSO-like variability on interannual time scales is expected without the Bjerknes feedback via thermodynamic coupling between the ocean and atmosphere [as previously suggested by Hameed et al. (1989), Zhou and Carton (1998), Kitoh et al. (1999), Chang et al. (2007), and Dommenget (2010)], and the TCW mechanism may contribute to the development of ENSO events. Furthermore, this mode of variability is a robust feature of all AGCM-slab models.

b. Decadal time scale

The slab model results show that variability in the SO can be expected on decadal time scales as a result of weak damping. Some models, such as the MRI, simulate variability out to multidecadal time scales, perhaps because of a positive cloud feedback (Kitoh et al. 1999). Inclusion of a larger ocean heat capacity (beyond a 50-m mixed layer) could introduce variability on even longer time scales, as has been illustrated by Dommenget and Latif (2008). On the other hand, interactive ocean dynamics in some coupled models (e.g., GFDL and MPI) can also produce enhanced power in the SO on decadal time scales relative to their slab components through a rectified effect of the interannual time-scale variability (Newman et al. 2003; Rodgers et al. 2004; Vimont 2005; van Oldenburg et al. 2005; An et al. 2007; Philip and van Oldenborgh 2009). These results suggest that the power

in the SO at decadal time scales can be thought of as being the combination of multiple processes: mixed layer integration of stochastic forcing (with weak damping) and a possible rectification of strong, nonlinear interannual variability. However, the balance of these processes is quite model dependent, and hence it is important to provide some observational constraints on the processes. In particular, to the extent that damping rates in the eastern Pacific basin may depend on low-cloud feedback (as suggested in Park et al. 2005), and that low-level clouds are poorly simulated by these models (Clement et al. 2009), the effective damping rate (and hence the persistence of SST and Walker circulation anomalies) in these models may be significantly in error.

One way that the spectral properties of the SO could be determined is with paleoclimate proxies, which can provide information about how damped the real-world Walker circulation is. For example, Ault et al. (2009) use a collection of corals in the Indo-Pacific to suggest that observational datasets underestimate the decadal variability in the nineteenth century. Lake records can provide an even longer temporal perspective, and one record from the Galapagos (Riedinger et al. 2002) suggests that the spectrum of the SO is red up to centennial and perhaps longer time scales. More paleoclimate records from the tropical Indo-Pacific are necessary to determine the temporal characteristics of "natural" variability in the SO. The South Pacific convergence zone (SPCZ) region appears to be important in carrying the low-frequency signals (Deser et al. 2004) and may be a good source for proxy information (Linsley et al. 2006).

We note here that the nonlocal nature of both thermodynamic and dynamical coupling makes them difficult to separate in the fully coupled system, and they may tend to compensate, as argued in Zhou and Carton (1995) and Jin et al. (2001). Thus, the AGCM-slab models may simulate weak thermal damping, while full coupling in nature will have a much stronger thermal damping. It is likely difficult, and even somewhat artificial, to attempt to unravel the separate effects of purely thermodynamic coupling from dynamical coupling in nature.

c. *Anthropogenic climate change*

As shown in a number of papers, the east–west gradient in equatorial Pacific SLP has been weakening over the twentieth century (Vecchi et al. 2006; Deser et al. 2010a), which has been attributed to the anthropogenically forced weakening of the Walker circulation. This has also been described as El Niño–like climate change (Meehl et al. 2007; Solomon et al. 2007). Our results suggest, however, that on decadal and longer time scales interactive ocean dynamics do not amplify climate anomalies as they do on interannual time scales. In fact, DiNezio et al. (2009) showed that in response to greenhouse gas forcing, all climate models simulate a shoaling and sharpening of the equatorial thermocline, which limits the warming in the eastern equatorial Pacific, actually acting as a negative feedback as previously suggested by Clement et al. (1996). Hence, the Bjerknes feedback does not appear to be a relevant mechanism for interpreting the adjustment of the Pacific climate to weaker trade winds due to anthropogenic forcing (DiNezio et al. 2010).

Finally, our findings have implications for the detection and attribution of anthropogenic changes to the Walker circulation. If the spectrum of natural variability in the SO is red up to multiple decades and longer, as occurs in some AGCM-slab models [e.g., MRI and CCSM, and as shown in Dommenget and Latif (2008)] and appears in some proxies (e.g., Riedinger et al. 2002; Ault et al. 2009), then detection is likely to be exceedingly difficult. In that case large ensemble sizes would be recommended to properly attribute SO changes (Deser et al. 2010b).

5. Conclusions

We have revisited the explanation of the Southern Oscillation (SO) without presuming a role for interactive ocean dynamics in its spatial and temporal characteristics. Our main finding is that models can simulate variability in the tropical Pacific climate that has the spatial structure of the SO without dynamical coupling to the ocean. Simulations with the Community Atmosphere Model (CAM) show that in the absence of thermodynamic coupling to the ocean, the dominant mode of sea level pressure variability in the Pacific is a zonally symmetric structure, and the spectrum of this mode is white. Thermodynamic coupling to an ocean mixed layer produces a dominant SO mode of variability with a spectrum that is red, consistent with a stochastically forced, weakly damped process. This mode of variability, which we refer to as the TCW, appears to be tied to weakening and strengthening of the trade winds, which leads to an ENSO-like SST pattern, an east–west shift in convection in the central Pacific, a weakening of the Walker circulation, and global teleconnections. The effects of dynamical coupling with the ocean include increasing the amplitude of this mode on interannual time scales and altering the teleconnections to particular regions, including the North Pacific and equatorial Atlantic. Otherwise, the patterns in SLP, SST, and precipitation that arise in association with the TCW are in very good agreement with observations, and we conclude that the TCW is a mechanism for generating variability on interannual to decadal time scales in the global climate.

On a final note, the Bjerknes feedback has received much attention for its role in interannual climate variability associated with ENSO, and has been invoked to explain variability on longer time scales as well. For example, Dijkstra and Neelin (1995) invoke a ''climatological Bjerknes feedback'' to explain the warm pool–cold tongue configuration of the Pacific climate, and Clement et al. (1996) argue that the Bjerknes feedback is important in the adjustment of the tropical Pacific to external forcing. Our present results suggest that ENSO-like variability can be produced without this feedback, and that the Bjerknes feedback only operates as a positive feedback on interannual time scales. Hence, the application of this conceptual feedback is not appropriate for interpreting decadal variability of anthropogenically forced climate change in the Pacific (DiNezio et al. 2010). Moreover, although we have adopted the terminology ''ENSO like'' in this paper to be consistent with the current literature, this study clearly demonstrates that the TCW is not ENSO like in its mechanism since there is no role for interactive ocean dynamics. However, the spatial structure of the climate variability of the TCW is very much ENSO like, which again suggests that ENSO-like climate changes need not be explained as resulting from the Bjerknes feedback.

Acknowledgments. The authors gratefully acknowledge Robert Tomas and Adam S. Phillips (NCAR) for their help in generating and making available model output. We would also like to thank Ben Kirtman, Walt Robinson, and Jerry Meehl for their insights. Thanks also go to Peter Gent for the reminder of how inappropriate the ''ENSO like'' terminology is with respect to mechanisms of low-frequency Pacific climate variability and change, and to Dallas Murphy for his encouragement. We acknowledge the various international modeling groups participating in Coupled Model Intercomparison Project Phase 3 (CMIP3). AC is funded by an NSF ATM grant (AGS0946225), a NOAA grant (NA10OAR4310204), and a DOE grant (DESC0004897). NCAR is sponsored by the National Science Foundation.

REFERENCES

Adler, R. F., and Coauthors, 2003: The version-2 Global Precipitation Climatology Project (GPCP) monthly precipitation analysis (1979–present). *J. Hydrometeor.,* **4,** 1147–1167.

Allen, R. J., and T. J. Ansell, 2006: A new globally complete monthly historical mean sea level pressure data set (HadSLP2): 1850–2004. *J. Climate,* **19,** 5816–5842.

An, S.-I., J.-S. Kug, A. Timmermann, I.-S. Kang, and O. Timm, 2007: The influence of ENSO on the generation of decadal variability in the North Pacific. *J. Climate,* **20,** 667–680.

Ault, T. R., J. E. Cole, M. N. Evans, H. Barnett, N. J. Abram, A. W. Tudhope, and B. K. Linsley, 2009: Intensified decadal variability in tropical climate during the late 19th century. *Geophys. Res. Lett.,* **36,** L08602, doi:10.1029/2008GL036924.

Barnett, T. P., D. W. Pierce, M. Latif, D. Dommenget, and R. Saravanan, 1999: Interdecadal interactions between the tropics and midlatitudes in the Pacific basin. *Geophys. Res. Lett.,* **26,** 615–618.

Barsugli, J. J., and D. S. Battisti, 1998: The basic effects of atmosphere–ocean thermal coupling on midlatitude variability. *J. Atmos. Sci.,* **55,** 477–493.

Bjerknes, J., 1969: Atmospheric teleconnections from the equatorial Pacific. *Mon. Wea. Rev.,* **97,** 163–172.

Cane, M. A., and E. S. Sarachik, 1977: Forced baroclinic ocean motions. Part II: The linear equatorial bounded case. *J. Mar. Res.,* **35,** 395–432.

Chang, P., and Coauthors, 2006: Climate fluctuations of tropical coupled systems—The role of ocean dynamics. *J. Climate,* **19,** 5122–5174.

——, L. Zhang, R. Saravanan, D. J. Vimont, J. C. H. Chiang, L. Ji, H. Seidel, and M. K. Tippett, 2007: Pacific meridional mode and El Niño–Southern Oscillation. *Geophys. Res. Lett.,* **34,** L16608, doi:10.1029/2007GL030302.

Chiang, J. C. H., and D. J. Vimont, 2004: Analogous Pacific and Atlantic meridional modes of tropical atmosphere–ocean variability. *J. Climate,* **17,** 4143–4158.

Clarke, A. J., 2010: Analytical theory for the quasi-steady and low-frequency equatorial ocean response to wind forcing: The ''tilt'' and ''warm water volume'' modes. *J. Phys. Oceanogr.,* **40,** 121–137.

Clement, A. C., R. Seager, M. A. Cane, and S. E. Zebiak, 1996: An ocean dynamical thermostat. *J. Climate,* **9,** 2190–2196.

——, ——, and R. Murtugudde, 2005: Why are there tropical warm pools? *J. Climate,* **18,** 5294–5311.

——, R. Burgman, and J. Norris, 2009: Model and observational evidence for positive low-level cloud feedback. *Science,* **325,** 460–464, doi:10.1126/science.1171255.

Collins, W. D., and Coauthors, 2006a: The Community Climate System Model version 3 (CCSM3). *J. Climate,* **19,** 2122–2143.

——, and Coauthors, 2006b: The formulation and atmospheric simulation of the Community Atmosphere Model version 3 (CAM3). *J. Climate,* **19,** 2144–2161.

Deser, C., A. Phillips, and J. Hurrell, 2004: Pacific interdecadal climate variability: Linkages between the tropics and North Pacific during boreal winter since 1900. *J. Climate,* **17,** 3109–3128.

——, A. Capotondi, R. Saravanan, and A. S. Phillips, 2006: Tropical Pacific and Atlantic climate variability in CCSM3. *J. Climate,* **19,** 2451–2481.

——, A. S. Phillips, and M. A. Alexander, 2010a: Twentieth century tropical sea surface temperature trends revisited. *Geophys. Res. Lett.,* **37,** L10701, doi:10.1029/2010GL043321.

——, ——, V. Bourdette, and H. Teng, 2010b: Uncertainty in climate change projections: The role of internal variability. *Climate Dyn.,* doi:10.1007/s00382-010-0977-x.

Dijkstra, H. A., and J. D. Neelin, 1995: Ocean–atmosphere interaction and the tropical climatology. Part II: Why the Pacific cold tongue is in the east. *J. Climate,* **8,** 1343–1359.

DiNezio, P. N., A. Clement, G. Vecchi, B. Soden, B. Kirtman, and S.-K. Lee, 2009: Climate response of the equatorial Pacific to global warming. *J. Climate,* **22,** 4873–4892.

——, ——, and ——, 2010: Tropical Pacific climate change: Reconciling models and observations. *Eos, Trans. Amer. Geophys. Union,* **91,** 141–142.

Dommenget, D., 2010: A slab ocean El Nino. *Geophys. Res. Lett.,* **37,** L20701, doi:10.1029/2010GL044888.

——, and M. Latif, 2008: Generation of hyper climate modes. *Geophys. Res. Lett.,* **35,** L02706, doi:10.1029/2007GL031087.

Du, Y., and S.-P. Xie, 2008: Role of atmospheric adjustments in the tropical Indian Ocean warming during the 20th century in climate models. *Geophys. Res. Lett.,* **35,** L08712, doi:10.1029/2008GL033631.

Frankignoul, C., and K. Hasselmann, 1977: Stochastic climate models. Part 2. Application to sea-surface temperature variability and thermocline variability. *Tellus,* **29,** 284–305.

Gu, D., and S. G. H. Philander, 1997: Internal climate fluctuations that depend on exchanges between the tropics and extratropics. *Science,* **275,** 805–807.

Guilyardi, E., 2006: El Niño–mean state–seasonal cycle interactions in a multi-model ensemble. *Climate Dyn.,* **26,** 329–348, doi:10.1007/s00382-005-0084-6.

Hameed, S., K. R. Sperber, and R. D. Cess, 1989: Genesis of the Southern Oscillation in the atmosphere: Illustration with global general circulation models. *Geophys. Res. Lett.,* **16,** 691–694.

Hare, S. R., and N. J. Mantua, 2000: Empirical evidence for North Pacific regime shifts in 1977 and 1989. *Prog. Oceanogr.,* **47,** 103–145.

Hastenrath, S., and L. Heller, 1977: Dynamics of climatic hazards in northeast Brazil. *Quart. J. Roy. Meteor. Soc.,* **103,** 77–92.

Hazeleger, W., R. Seager, M. Visbeck, N. Naik, and K. Rodgers, 2001: Impact of the midlatitude storm track on the upper Pacific Ocean. *J. Phys. Oceanogr.,* **31,** 616–636.

——, C. Severijns, R. Seager, and F. Molteni, 2005: Tropical Pacific-driven decadal energy transport variability. *J. Climate,* **18,** 2037–2051.

Hulme, M., T. J. Osborn, and T. C. Collins, 1998: Precipitation sensitivity to global warming: Comparison of observations with HadCM2 simulations. *Geophys. Res. Lett.,* **25,** 3379–3382.

Hurrell, J. W., J. J. Hack, D. Shea, J. M. Caron, and J. Rosinski, 2008: A new sea surface temperature and sea ice boundary dataset for the Community Atmosphere Model. *J. Climate,* **21,** 5145–5153.

Jin, F.-F., 1997: An equatorial ocean recharge paradigm for ENSO. Part I: Conceptual model. *J. Atmos. Sci.,* **54,** 811–829.

——, and J. D. Neelin, 1993: Modes of interannual tropical ocean–atmosphere interaction—A unified view. Part I: Numerical results. *J. Atmos. Sci.,* **50,** 3477–3503.

——, Z.-Z. Hu, M. Latif, L. Bengtsson and E. Roeckner, 2001: Dynamical and cloud–radiation feedbacks in El Niño and greenhouse warming. *Geophys. Res. Lett.,* **28,** 1539–1542.

Karspeck, A., and M. Cane, 2002: Tropical Pacific 1976–77 climate shift in a linear, wind-driven model. *J. Phys. Oceanogr.,* **32,** 2350–2360.

Kitoh, A., T. Motoi, and H. Koide, 1999: SST variability and its mechanism in a coupled atmosphere–mixed-layer ocean model. *J. Climate,* **12,** 1221–1239.

Kwon, Y.-O., C. Deser, and C. Cassou, 2010: Coupled atmosphere–mixed layer ocean response to ocean heat flux convergence along the Kuroshio current extension. *Climate Dyn.,* doi:10.1007/s00382-010-0764-8.

Latif, M., and T. P. Barnett, 1994: Causes of decadal climate variability over the North Pacific and North America. *Science,* **266,** 634–637.

Linsley, B. K., A. Kaplan, Y. Gouriou, J. Salinger, P. B. deMenocal, G. M. Wellington, and S. S. Howe, 2006: Tracking the extent of the South Pacific convergence zone since the early 1600s. *Geochem. Geophys. Geosyst.,* **7,** Q05003, doi:10.1029/2005GC001115.

Lloyd, J., E. Guilyardi, and H. Weller, 2010: The role of atmosphere feedbacks during ENSO in the CMIP3 models. Part II: Using AMIP runs to understand the heat flux feedback mechanisms. *Climate Dyn.,* doi:10.1007/s00382-010-0895-y.

Mantua, N. J., S. R. Hare, Y. Zhang, J. M. Wallace, and R. C. Francis, 1997: A Pacific interdecadal climate oscillation with impacts on salmon production. *Bull. Amer. Meteor. Soc.,* **78,** 1069–1079.

Meehl, G. A., and Coauthors, 2007: Global climate projections. *Climate Change 2007: The Physical Science Basis,* S. Solomon et al., Eds., Cambridge University Press, 747–846.

Minobe, S., 1997: A 50–70-year climatic oscillation over the North Pacific and North America. *Geophys. Res. Lett.,* **24,** 683–686.

Neelin, J. D., 1991: The slow sea surface temperature mode and the fast-wave limit: Analytic theory for tropical interannual oscillations and experiments in a hybrid coupled model. *J. Atmos. Sci.,* **48,** 584–606.

——, D. S. Battisti, A. C. Hirst, F.-F. Jin, Y. Wakata, T. Yamagata, and S. E. Zebiak, 1998: ENSO theory. *J. Geophys. Res.,* **103** (C7), 14 261–14 290.

Newman, M., G. P. Compo, and M. A. Alexander, 2003: ENSO-forced variability of the Pacific decadal oscillation. *J. Climate,* **16,** 3853–3857.

Oleson, K. W., and Coauthors, 2004: Technical description of the Community Land Model (CLM). NCAR Tech. Note NCAR/TN-461+STR, 173 pp.

Park, S., C. Deser, and M. A. Alexander, 2005: Estimation of the surface heat flux response to sea surface temperature anomalies over the global oceans. *J. Climate,* **18,** 4582–4599.

Penland, C., and P. D. Sardeshmukh, 1995: The optimal growth of tropical sea surface temperature anomalies. *J. Climate,* **8,** 1999–2024.

Peterson, W. T., and F. B. Schwing, 2003: A new climate regime in northeast Pacific ecosystems. *Geophys. Res. Lett.,* **30,** 1896, doi:10.1029/2003GL017528.

Philip, S. Y., and G. J. van Oldenborgh, 2009: Significant atmospheric nonlinearities in the ENSO cycle. *J. Climate,* **22,** 4014–4028.

Pierce, D. W., T. P. Barnett, and M. Latif, 2000: Connections between the Pacific Ocean tropics and midlatitudes on decadal timescales. *J. Climate,* **13,** 1173–1194.

——, ——, N. Schneider, R. Saravanan, D. Dommenget, and M. Latif, 2001: The role of ocean dynamics in producing decadal climate variability in the North Pacific. *Climate Dyn.,* **18,** 51–70.

Rayner, N. A., and Coauthors, 2003: Global analyses of sea surface temperature, sea ice, and night marine air temperature since the late nineteenth century. *J. Geophys. Res.,* **108,** 4407, doi:10.1029/2002JD002670.

Riedinger, M. A., M. Steinitz-Kannan, W. M. Last, and M. Brenner, 2002: A ~6100 ^{14}C yr record of El Niño activity from the Galápagos Islands. *J. Paleolimnol.,* **27,** 1–7.

Rodgers, K. B., P. Friederichs, and M. Latif, 2004: Tropical Pacific decadal variability and its relation to decadal modulation of ENSO. *J. Climate,* **17,** 3761–3774.

Saravanan, R., and P. Chang, 2000: Interactions between the Pacific ENSO and tropical Atlantic climate variability. *J. Climate,* **13,** 2177–2194.

Schubert, S. D., M. J. Suarez, P. J. Pegion, R. D. Koster, and J. T. Bacmeister, 2004: On the cause of the 1930s Dust Bowl. *Science,* **303,** 1855–1859.

Seager, R., R. Murtugudde, N. Naik, A. C. Clement, N. Gordon, and J. Miller, 2003: Air–sea interaction and the seasonal cycle of the subtropical anticyclones. *J. Climate,* **16,** 1948–1966.

——, Y. Kushnir, C. Herweijer, N. Naik, and J. Velez, 2005: Modeling of tropical forcing of persistent droughts and pluvials over western North America: 1856–2000. *J. Climate,* **18,** 4065–4088.

Smith, T. M., R. W. Reynolds, T. C. Peterson, and J. Lawrimore, 2008: Improvements to NOAA's historical merged land–ocean surface temperature analysis (1880–2006). *J. Climate,* **21,** 2283–2296.

Solomon, S., D. Qin, M. Manning, M. Marquis, K. Averyt, M. M. B. Tignor, H. L. Miller Jr., and Z. Chen, Eds., 2007: *Climate Change 2007: The Physical Science Basis*. Cambridge University Press, 996 pp.

Terray, P., 2010: Southern Hemisphere extratropical forcing: A new paradigm for El Niño–Southern Oscillation. *Climate Dyn.,* doi:10.1007/s00382-010-0825-z.

Trenberth, K. E., and J. M. Caron, 2000: The Southern Oscillation revisited: Sea level pressures, surface temperatures, and precipitation. *J. Climate,* **13,** 4358–4365.

Troupe, A. J., 1965: The Southern Oscillation. *Quart. J. Roy. Meteor. Soc.,* **91,** 490–506.

Van Loon, H., and D. J. Shea, 1985: The Southern Oscillation. Part IV. The precursors south of 15°S to the extremes of the oscillation. *Mon. Wea. Rev.,* **113,** 2063–2074.

van Oldenborgh, G. J., S. Y. Philip and M. Collins, 2005: El Niño in a changing climate: A multi-model study. *Ocean Sci.,* **1,** 81–95.

Vecchi, G. A., and B. J. Soden, A. T. Wittenberg, I. M. Held, A. Leetmaa, and M. J. Harrison, 2006: Weakening of tropical Pacific atmospheric circulation due to anthropogenic forcing. *Nature,* **441,** 73–76, doi:10.1038/nature04744.

Vimont, D. J., 2005: The contribution of the interannual ENSO cycle to the spatial pattern of decadal ENSO-like variability. *J. Climate,* **18,** 2080–2092.

——, J. M. Wallace, and D. S. Battisti, 2003: The seasonal footprinting mechanism in the Pacific: Implications for ENSO. *J. Climate,* **16,** 2668–2675.

Walker, G., 1924: Correlations in seasonal variations in weather IX: A further study of world weather. *Mem. Ind. Meteor. Dept.,* **24,** 275–322.

Wyrtki, K., 1975: El Niño—The dynamic response of the equatorial Pacific Ocean to atmospheric forcing. *J. Phys. Oceanogr.,* **5,** 572–584.

Yeh, S.-W., and B. P. Kirtman, 2006: Origin of decadal El Niño–Southern Oscillation-like variability in a coupled general circulation model. *J. Geophys. Res.,* **111,** C01009, doi:10.1029/2005JC002985.

Zebiak, S. E., and M. A. Cane, 1987: A model El Nino–Southern Oscillation. *Mon. Wea. Rev.,* **115,** 2262–2278.

Zhang, Y., J. M. Wallace, and D. S. Battisti, 1997: ENSO-like interdecadal variability: 1900–93. *J. Climate,* **10,** 1004–1020.

Zhou, Z., and J. A. Carton, 1998: Latent heat flux and interannual variability of the coupled atmosphere–ocean system. *J. Atmos. Sci.,* **55,** 494–501.